

Expectation values from any quantum measurement

Dominik Šafránek^{1,*} and Dario Rosa^{1,2,†}

¹*Center for Theoretical Physics of Complex Systems,*

Institute for Basic Science (IBS), Daejeon - 34126, Korea

²*Basic Science Program, Korea University of Science and Technology (UST), Daejeon - 34113, Korea*

(Dated: April 7, 2023)

We present a method to estimate the probabilities of outcomes of an observable, its mean value, and higher moments, by measuring any other observable. This method is general and can be applied to any quantum system. In the case of estimating the mean energy of an isolated system, the estimate can be further improved by measuring the other observable at different times. Intuitively, this method uses interplay and correlations between the measured and the estimated observable, and the state of the system. We provide two bounds: one that is looser but analytically computable, and one that is tighter but requires solving a non-convex optimization problem. The method can be used to estimate expectation values and related quantities such as temperature and work in setups in which performing measurements in a highly entangled basis is difficult, finding use in state-of-the-art quantum simulators. As a demonstration, we show that in Heisenberg and Ising models of ten sites in the localized phase, performing two-qubit measurements excludes 97.5% and 96.7% of the possible range of energies, respectively, when estimating the ground state energy.

I. INTRODUCTION

Expectation values are ubiquitous in quantum physics, characterizing different types of behaviors of quantum systems. They are used both as descriptive and predictive tools. To name several: mean values of generic local observables classify many-body systems according to how well they thermalize [1, 2]. Vanishing total magnetization identifies a quantum phase transition [3–5]. The mean value of homodyne measurement [6–9] is evaluated in magnetic resonance imaging [10] and quantum cryptography protocols [11], while its variance is used to prove squeezing [12, 13] — an essential resource for quantum sensors [14]. Variances also appear in Heisenberg’s uncertainty principle [15–17]. Expectation values are the object of interest in quantum field theory [18, 19] and in nuclear physics [20, 21].

Moments of energy are somewhat special due to their wide range of applications. The mean energy determines the thermodynamic entropy of the system [22–25] and its temperature [26–28]. Its change may represent heat and work [29–34] and its difference defines a measure of extractable work called ergotropy [35–37]. Variance in energy determines the precision in estimating both the time [38] and temperature [39] parameters. Both moments, when combined, provide a tight bound on the characteristic time scale of a quantum system [40–42].

Given the breadth of applications, it is clear that measuring and estimating expectation values is of essential importance. This may be however challenging. In quantum many-body systems, the mean energy is considerably difficult to measure, with only a few architecture-specific proposals [43] and experiments [44] known. This

is because energy eigenstates are typically highly entangled. In quantum simulators, measuring in an entangled basis is performed by combining a number of elementary gates. Each gate has a fixed fidelity, and when many of such gates are combined, the fidelity diminishes making such measurements unreliable [45–48]. Additionally, experimental setups may allow measurement only of a close but not the exact observable that we are interested in. This is the case for example in the aforementioned homodyne detection with a finite, instead of infinite, oscillator field strength [7, 49].

In this paper, we show that performing any measurement gives a bound on the mean value and higher moments of *any other* observable. The bound is further tightened by measuring in different bases and, in the case of estimating the mean energy, by measuring at different times. After some preliminaries, we show how measurement in any basis bounds the probabilities of the system to have a certain mean energy. From this, we derive two bounds on the mean value of energy: one analytic which is easy to compute, and one tighter which leads to an optimization problem. We discuss situations in which the analytic bound becomes relatively tight. Then we describe a few differences when bounding the mean values of observables other than energy. We illustrate this method on a number of experimentally relevant models. Finally, we discuss the advantages and drawbacks of this method, possible applications, and future directions.

II. RESULTS

Setup. Consider any quantum system and a measurement given by the measurement basis $\mathcal{C} = \{|i\rangle\}$. Label i is the outcome of the measurement, and the probability of obtaining the outcome at time t is $p_i = |\langle i|\psi_t\rangle|^2$. $|\psi_t\rangle$ is the state of the system at time t . If we create many realiza-

* dsafranekibs@gmail.com

† dario_rosa@ibs.re.kr

tions of the same experiment by repeating the sequence prepare-and-measure, we can build the statistics of outcomes and determine the probability distribution $\{p_i\}$. Thus, these probabilities are experimentally accessible.

Next, we consider a Hamiltonian of the system, with spectral decomposition in terms of its eigenvalues and eigenvectors being $\hat{H} = \sum_E E |E\rangle\langle E|$. The probability of finding the system having energy E is given by $p_E = |\langle E|\psi_t\rangle|^2$. We assume to know the Hamiltonian and its spectral decomposition. However, we presume that we are unable to measure it experimentally. In other words, we cannot perform the measurement in the energy eigenbasis. As we will show next, this does not stop us from estimating its probability of outcomes, and from those also the mean value of energy.

Bounds on energy probabilities. The key result of this paper is that one finds the probability of the state having energy E between two bounds,

$$a_E \leq p_E \leq b_E, \quad (1)$$

where

$$\begin{aligned} a_E &= \max \left\{ 2 \sum_i c_{iE}^2 - b_E, 0 \right\}, \\ b_E &= \left(\sum_i c_{iE} \right)^2, \end{aligned} \quad (2)$$

and $c_{iE} = \sqrt{p_i} |\langle i|E\rangle|$. This element contains both the probability of outcome, p_i , and the correlation between the measured and the estimated observable, given by overlap $|\langle i|E\rangle|$. Thus, the above inequality connects the probability of the estimated observable to the probability of the measured observable, through the correlations between their eigenbases. We can easily derive that $b_E \leq 1$ from the Cauchy-Schwarz inequality. Thus, the upper bound on the energy probability is always non-trivial.

If the system is isolated, it evolves unitarily with the time-independent Hamiltonian \hat{H} , and energy probabilities p_E are also time-independent. In contrast, probabilities p_i are time-dependent if the measurement basis does not commute with the Hamiltonian, and so are the bounds a_E and b_E . This leads to an interesting observation that measuring at different times can make the bound tighter. Quantitatively, we have

$$a_E^{\max} \leq p_E \leq b_E^{\min}, \quad (3)$$

where $a_E^{\max} = \max_{t \in [0, T]} a_E$ and $b_E^{\min} = \min_{t \in [0, T]} b_E$.

Let us discuss situations in which the bound becomes tight. First, assume that one of the measurement basis vectors is an energy eigenvector, i.e., $|i\rangle = |E\rangle$ for some i and E . Then the bound gives $p_E = p_i$ for this specific E , as intuitively expected. Second, consider a situation in which we always obtain a single outcome when measuring at a specific time, i.e., $p_i = 1$ for some i at some time t . Doing this is akin to identifying the state of the system as being equal to $|i\rangle$. As a result, the bound gives an identity $p_E = |\langle i|E\rangle|$ for all energies E so the entire energy distribution is determined exactly.

The two extreme cases just discussed suggest two possible scenarios in which the bounds perform well. The bounds are relatively tight when either the measurement basis resembles the eigenbasis of the estimated observable (in this case, the Hamiltonian), or when the state of the system comes close to one of the measurement basis vectors during its time evolution.

In addition to optimization over time, the inequalities can be further tightened by performing measurements in different bases. Defining a set of performed measurements, $\mathcal{M} = \{\mathcal{C}_m\}$, each measurement bounds the p_E independently, so we can take

$$a_E^{\max} = \max_{\mathcal{C}_m \in \mathcal{M}, t \in [0, T]} a_E^m, \quad b_E^{\min} = \min_{\mathcal{C}_m \in \mathcal{M}, t \in [0, T]} b_E^m, \quad (4)$$

for the bound (3). $a_E^m(t)$ and $b_E^m(t)$ are defined by Eqs. (2) for each measurement \mathcal{C}_m . This may be helpful when there are limits on the types of measurements we can perform. For example, we can be experimentally limited to using only one- and two-qubit gates, due to many-qubit gates having a low fidelity.

Bounds on collections of energy probabilities. Additionally, we derive the following collective bounds on the energy probabilities,

$$\sqrt{\mathbf{p}}^T \mathbf{A}_i \sqrt{\mathbf{p}} \leq p_i \leq \sqrt{\mathbf{p}}^T \mathbf{B}_i \sqrt{\mathbf{p}}. \quad (5)$$

The left and the right-hand sides are time-independent quadratic forms, which are defined by their elements as

$$\begin{aligned} (\mathbf{A}_i)_{EE'} &= (-1)^{1+\delta_{EE'}} |\langle E|i\rangle\langle i|E'\rangle|, \\ (\mathbf{B}_i)_{EE'} &= |\langle E|i\rangle\langle i|E'\rangle|. \end{aligned} \quad (6)$$

They are applied on the vector of the square root of energy probabilities $\sqrt{\mathbf{p}}_E = \sqrt{p_E}$, which are those that we would like to estimate.

For the Hamiltonian evolution, extremizing over times of measurement yields tighter bounds

$$\sqrt{\mathbf{p}}^T \mathbf{A}_i \sqrt{\mathbf{p}} \leq p_i^{\min} \leq p_i^{\max} \leq \sqrt{\mathbf{p}}^T \mathbf{B}_i \sqrt{\mathbf{p}}, \quad (7)$$

where $p_i^{\min} = \min_{t \in [0, T]} p_i$ and $p_i^{\max} = \max_{t \in [0, T]} p_i$.

These collective inequalities are generally non-linear in p_E and neither convex nor concave. There are as many as the number of measurement outcomes. While they do not bound each energy probability separately, they provide relationships between their respective sizes. For example, one can derive quantitative statements of type: if p_{E_1} is high, then p_{E_2} must be low. They might require numerical methods to work with due to their non-linearity. However, they can provide a powerful improvement in estimating energy in some cases. See Supplemental Material for such an example of coarse-grained energy measurements.

Similar to Eq. (4), one can employ measurements in different bases. These generate more conditions for probabilities p_E of type (7), thus making quantitative relations between them stricter.

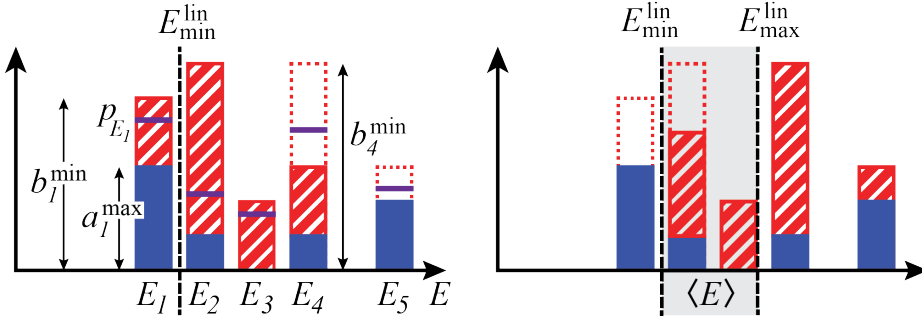


FIG. 1. **Bounds on energy probabilities and on the mean energy.** Each energy probability p_{E_l} is bounded by a_l^{\max} from below and by b_l^{\min} from above. The analytical bound on the mean energy is computed as follows: the lower bound (left figure) is found by filling the minimal probability of each energy given by a_l^{\max} (blue solid), and topping it up to the maximum b_l^{\min} (red striped), from the lowest to the highest energy, until the probabilities sum up to one. The upper bound (right figure) is obtained by the same method, but going from the highest to the lowest energy. The mean energy $\langle E \rangle$ lies somewhere in the shaded region.

Bounds on the mean energy. Given the derived bounds on the probability distribution of energy, we can bound the mean energy of the system as follows,

$$E_{\min}^{\text{lin}} \leq E_{\min} \leq \langle E \rangle \leq E_{\max} \leq E_{\max}^{\text{lin}}. \quad (8)$$

The inner bound is tighter but may be difficult to compute. The outer bound is looser but it is analytically computable.

The inner bound is computed by optimizing the mean value of energy, $\langle E \rangle = \sum_E E p_E$, as

$$E_{\min} = \min_{\{p_E\} \in S} \langle E \rangle, \quad E_{\max} = \max_{\{p_E\} \in S} \langle E \rangle, \quad (9)$$

over the set of probability distributions consistent with our observations, i.e., over the set that satisfies all the required inequalities

$$S = \left\{ \{p_E\} \left| \sum_E p_E = 1, \text{ Eq. (3), and Eq. (7)} \right. \right\}. \quad (10)$$

The mean energy itself is a linear function. While $\sum_E p_E = 1$ and Eq. (3) are linear constraints, Eq. (7) is in general non-linear. Computing E_{\min} and E_{\max} is therefore a non-linear constrained optimization problem. These problems are considered to be computationally demanding, although they are difficult to characterize within computational complexity theory [50]. They can be solved only approximately by various methods [51–57]. Time to find an exact solution typically scales exponentially with the number of variables, in our case, the dimension of the system.

However, we can solve an easier problem by including only linear constraints in the optimization, i.e., by removing the requirement for satisfying Eqs. (7). This makes the bound looser but it allows for solving this optimization problem analytically. We assume that energy eigenvalues are ordered in increasing order as $E_j \leq E_{j+1}$

with E_1 representing the ground state energy. We have

$$E_{\min}^{\text{lin}} = \sum_{j=1}^N E_j u_j, \quad (11)$$

where probabilities $u_j \equiv u_{E_j}$ are computed recursively starting from the ground state as

$$u_1 = \min \left\{ b_1^{\min}, 1 - \sum_{l=2}^N a_l^{\max} \right\}, \quad (12)$$

$$u_j = \min \left\{ b_j^{\min}, 1 - \sum_{l=1}^{j-1} u_l - \sum_{l=j+1}^N a_l^{\max} \right\}, \quad 2 \leq j \leq N.$$

(We simplified lower indices as $l \equiv E_l$ and the dimension of the system is N .) Similarly, we obtain

$$E_{\max}^{\text{lin}} = \sum_{j=1}^N E_j w_j, \quad (13)$$

where, starting from the highest energy state, we have

$$w_N = \min \left\{ b_N^{\min}, 1 - \sum_{l=1}^{N-1} a_l^{\max} \right\}, \quad (14)$$

$$w_j = \min \left\{ b_j^{\min}, 1 - \sum_{l=j+1}^N w_l - \sum_{l=1}^{j-1} a_l^{\max} \right\}, \quad 1 \leq j \leq N-1.$$

The reasoning behind this derivation is explained in Fig. 1 and performed in detail in the Supplemental Material. Bounds for the higher moments are computed by replacing eigenvalues E with E^k in Eq. (9).

Tightness of the analytic bound on the mean value of energy. Below Eq. (3), we discussed two cases where the bound on the energy probability distribution becomes tight. Now we show that the same arguments can be also extended to discuss the tightness of the bound on the mean energy, Eq. (8).

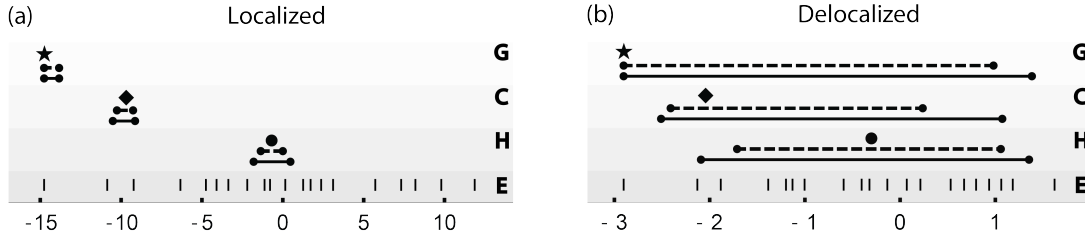


FIG. 2. **Heisenberg model in the localized and the delocalized phases, 3 particles on 6 sites.** Estimating energy by measuring in the local number basis (corresponding to $k = 0$ in Fig. 3). The initial state is either a ground state (G), a cold state (C), Eq. (17), or a hot state (H). The graphs show the true mean energy $\langle E \rangle$ (single symbols—star, diamond, and disc for G, C, and H, respectively), intervals of analytic bounds $[E_{\min}^{\text{lin}}, E_{\max}^{\text{lin}}]$ (full lines) and numerical bounds $[E_{\min}, E_{\max}]$ (dashed lines) for each state. We also plot the list of energy eigenvalues at the very bottom (E). In the localized phase, energy eigenstates have a large overlap with the local number basis, making the energy estimation significantly more precise.

The first case is when the state of the system comes close to one of the measurement basis vectors during its time evolution. Clearly, if the state becomes exactly one of the basis vectors, i.e., $p_i(t) = 1$ at some time t , we can identify the state exactly as $|i\rangle$ and so all of its properties, energy included. In this case, bounds (3) become tight and we obtain $\langle E \rangle = E_{\max}^{\text{lin}} = E_{\min}^{\text{lin}}$. The most informative times of measurement are those of a low value of observational entropy [25, 58–62], due to the state wandering into a small subspace of the Hilbert space [25, 63] recognizable by the measurement. This can be of advantage for energy estimation in systems that exhibit recurrences and Loschmidt echo [64–68], which return close to their original state after some time.

The second is when the measurement is close to the energy measurement itself. This happens for example in the localized phase of many-body localized systems, in which the energy eigenvectors tend to localize in small portions of the Fock space [69]. Thus, measuring local particle numbers is almost as good as measuring the energy itself. This is mathematically justified below Eq. (3).

Bounding the mean values of observables other than energy. The derivations and results above can be repeated as they are for any observable that commutes with the Hamiltonian. In that context, E would denote an eigenvalue of an observable other than energy. For observables that do not commute with the Hamiltonian, the procedure can be repeated but it must be performed only at a fixed time t (extremization over time, Eqs. (3) and (7), is not possible). Extremization over different measurements at a fixed time, Eqs. (4), can be employed.

Demonstration on experimentally relevant many-body systems. We numerically demonstrate this method on the paradigmatic example of the one-dimensional disordered Heisenberg model [70–72]. Numerical experiments for other experimentally achieved models, Ising [73–76], XY [77–80], and PXP models [81–83], and a simple analytical example are presented in the Supplemental Material.

The Hamiltonian is given by

$$\hat{H} = \sum_i (\hat{\sigma}_i^x \hat{\sigma}_{i+1}^x + \hat{\sigma}_i^y \hat{\sigma}_{i+1}^y + \hat{\sigma}_i^z \hat{\sigma}_{i+1}^z) + \sum_i h_i \hat{\sigma}_i^z, \quad (15)$$

where $\hat{\sigma}_i^a$, $a = x, y, z$, are the Pauli operators acting at the site i . The constants h_i are randomly extracted within the interval $[-W, W]$ with W being the disorder strength. We show the case $W = 0.5$ for the chaotic (delocalized) regime and $W = 10$ for the localized regime [71, 72]. See Supplemental Material for the Bethe integrable regime $W = 0$ [84].

We choose a complete measurement in the local number basis,

$$\mathcal{C} = \{|i_1\rangle \otimes \dots \otimes |i_L\rangle\}_{i_1, \dots, i_L}, \quad (16)$$

for small systems simulations. There, $i_j = 0, 1$ for all j , and L is the length of the chain (such that the dimension of the Hilbert space is $N = 2^L$). For large system simulations, we also add optimized k -local measurements.

We consider three types of initial states: First the ground state (G). The second is a “pure thermal” state (C),

$$|\psi_\beta\rangle = \frac{1}{\mathcal{N}} \sum_E e^{-\beta E/2} |E\rangle, \quad (17)$$

where \mathcal{N} is the normalization factor and the inverse temperature is chosen as $\beta = 6/(E_N - E_1)$. We take this choice of β to imitate a cold state. Third, we choose a pure state chosen randomly from the Hilbert space with the Haar measure (H), imitating an infinite temperature state.

We evolve them with the Hamiltonian for the total time of $T = 160$ to compute the bounds.

In Figure 2, we show estimates of energy in small systems. We analytically solve for the looser bound using Eqs. (11) and (13). This solution serves as a starting point for the COBYLA optimization algorithm [57, 85] to compute the tighter bound, Eq. (9). In Figure 3, we plot estimates of energy in a large system, in which computing the numeric bound is prohibitively difficult. Instead, we

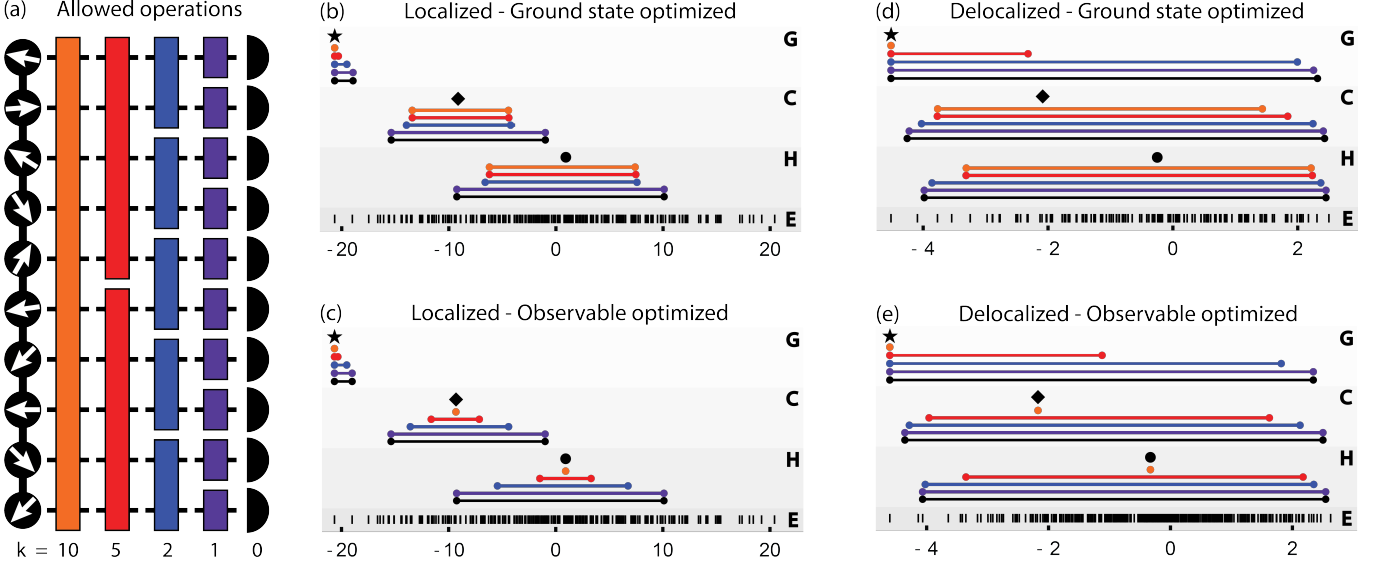


FIG. 3. **Heisenberg model in the localized and the delocalized phases, 5 particles on 10 sites.** Estimating energy with progressively added optimized k -local measurements, with the same initial states as in Fig. 2 (G,C,H) and energy eigenvalues plotted at the very bottom (E). In large systems, we can no longer employ numerical methods to improve the analytic bound. Instead, we employ different measurements. (a) Sketch of allowed operations. $k = 0$ (black) corresponds to measuring in the local number basis. $k = 1$ (purple) allows for using single-site unitary operators before measuring in the local number basis, which leads to a general single-site measurement, $k = 2$ (blue) allows for using two-site local operators, etc. (b) and (d): In the ground state optimized method, the measurement basis is given by the eigenbasis of the k -local reduced state of the ground state. Intervals of analytic bounds $[E_{\min}^{\text{lin}(k)}, E_{\max}^{\text{lin}(k)}]$ are labeled with the colors matching the allowed operations. (c) and (e): In the observable optimized method, the experimenter measures k -local blocks of the Hamiltonian. The observable-optimized method achieves perfect energy estimation for all initial states ($k = 10$ corresponds to measuring the Hamiltonian itself). In contrast, the ground state-optimized achieves that only for the ground state ($k = 10$ corresponds to measuring in a basis that contains the ground state). Using two-qubit measurements ($k = 2$) in the localized phase, the bound excludes 97.5% of the possible range of energies when estimating the ground state energy. See the Methods section for the descriptions of the ground state optimized and observable optimized methods. See Supplemental Material for details and for additional simulations of experimentally achievable XY, PXP, and Ising models.

add more measurements and compute the corresponding analytical bounds in the increasing degree of non-locality.

Generalization to mixed states and POVMs. Most general quantum measurements are represented by the positive operator-valued measure (POVM), $\mathcal{C} = \{\hat{\Pi}_i\}_i$, satisfying the completeness relation $\sum_i \hat{\Pi}_i = \hat{I}$. $\hat{\Pi}_i$ is a positive semi-definite operator called a POVM element. For a density matrix $\hat{\rho}$ representing the state of the system, the probability of obtaining measurement outcome i is given by $p_i = \text{tr}[\hat{\Pi}_i \hat{\rho}]$.

POVM elements admit a spectral decomposition $\hat{\Pi}_i = \sum_k \gamma_i^k |i^k\rangle\langle i^k|$. There, $0 < \gamma_i^k \leq 1$ and $|i^k\rangle$ are orthogonal to each other for different k 's. We define its “volume” as $V_i = \text{tr}[\hat{\Pi}_i]$. We further define $x_i^E = \min_k \gamma_i^k |\langle i^k | E \rangle|^2$, $y_i^E = \max_k |\langle i^k | E \rangle|^2$, and $\gamma_i = \min_k \gamma_i^k$. Note that these extrema are taken only over k for which γ_i^k is positive, i.e., non-zero.

The results of this paper generalize to mixed states and

general measurements by taking

$$a_E = \max \left\{ \sum_i p_i (x_i^E + \gamma_i y_i^E) - \left(\sum_i \sqrt{p_i y_i^E V_i} \right)^2, 0 \right\},$$

$$b_E = \left(\sum_i \sqrt{p_i \langle E | \hat{\Pi}_i | E \rangle} \right)^2, \quad (18)$$

in Eq. (1), and by taking

$$(\mathbf{A}_i)_{EE'} = (-1)^{1+\delta_{EE'}} |\langle E | \hat{\Pi}_i | E' \rangle|, \quad (19)$$

$$(\mathbf{B}_i)_{EE'} = |\langle E | \hat{\Pi}_i | E' \rangle|,$$

in Eq. (6). Results that come after do not depend on the specific form of the bounds, thus these proceed identically. For a complete projective measurement, we have $\hat{\Pi}_i = |i\rangle\langle i|$, which implies $x_i^E = y_i^E = |\langle i | E \rangle|^2$ and $\gamma_i = V_i = 1$, from which the initial bounds easily follow.

III. DISCUSSION

Quantum measurements provide more information than one would originally think. Measuring in the basis of one observable gives information on the distribution and expectation values of every other observable. The method works well either when the measured and the estimated observables resemble each other, or when the system state is close to one of the measurement basis states. On the other hand, if the measurement cannot distinguish between two eigenstates with very different eigenvalues, and the system state has a large overlap with one of them, the method naturally cannot give a good estimate. However, this can be overcome by combining measurements in different bases. Additionally, when estimating conserved quantities, better estimates are obtained by measuring at different times.

It is interesting to compare the presented method with the recent work of [86]. There, an algorithm is provided in which by applying random unitary operators it is possible to approximate the mean value of an observable with high probability. However, it is assumed that the set from which the unitary operators are drawn is *tomographically complete*, meaning it is possible to perform a full quantum tomography with it. This may be experimentally challenging because such a set must contain highly entangling operators. We do not require this assumption; any measurement will yield a bound making these results applicable to experiments, which are often limited in the types of measurements that can be performed.

We argued for using this method for estimating moments of energy, which have a wide range of applications while being difficult to measure directly in many-body systems. For instance, using this method one can bound the characteristic timescale through the Mandelstam-Tamm and Margolus-Levitin bounds [40–42], to estimate the amount of extractable work from an unknown source of states [37], or to estimate temperature. The latest can be used to benchmark the cooling function of quantum annealers [87–90] and adiabatic quantum computers [91]. This could be particularly suitable for systems with area-law entanglement scaling [69, 92], in which local measurements should be more powerful given the absence of long-range correlations in the eigenstates of such systems. We confirmed this numerically in two gapped models, which are proven to have area-law ground states [93]. In these, estimating the ground state energy using only local measurements works especially well. The method can also be used to prove entanglement through an entanglement witness (operator \hat{A}), without measuring the witness itself: to prove entanglement, it is enough to show that the expectation value of this operator is negative [94–96].

On a theoretical ground, this research instigates new possible paths of exploration. How to choose a measurement given some restriction, for example, on its locality or the number of elementary gates it consists of, that leads to the tightest possible bound? Is it possible to ap-

ply machine learning models to find this optimal strategy? Will the bound give an exact value, when the set of measurements is tomographically complete? Can this method be modified to identify the properties of channels, instead of states? Given that this method bounds the entire probability distribution of outcomes, is it possible to modify it to calculate estimates of functions of a state other than expectation values, such as entanglement entropy?

IV. METHODS

Ground state optimized and observable optimized methods for finding appropriate k -local measurements. We choose a chain of length $L = 10$ and two-local ($k = 2$) measurements to illustrate.

Ground state optimized method: This method is inspired by the Matrix Product State ansatz [97], and by the correspondence between observational and entanglement entropy [98]. We choose a pure state (in our case the ground state) $|\psi_0\rangle$ for which we want to optimize. We divide the chain into L/k local parts and generate the local basis as an eigenbasis of the reduced state. This corresponds to the local Schmidt basis. For example, for the first two sites denoted as subsystem A_1 , while denoting the full system as A , we have

$$\hat{A}_{A_1} = \text{tr}_{A \setminus A_1} |\psi_0\rangle\langle\psi_0|, \quad (20)$$

from which we compute eigenvectors $\{|\psi_{i_1}^{A_1}\rangle\}$. The final, ground state-optimized two-local measurement basis is given as a product of such generated local basis,

$$\{|\psi_{i_1}^{A_1}\rangle \otimes |\psi_{i_2}^{A_2}\rangle \otimes |\psi_{i_3}^{A_3}\rangle \otimes |\psi_{i_4}^{A_4}\rangle \otimes |\psi_{i_5}^{A_5}\rangle\}. \quad (21)$$

This method ensures that for the full system ($k = L$), the ground state is one of the measurement basis states.

Observable optimized method: This method is a k -local optimization for a specific observable, in our case the Hamiltonian. The basis is generated by the eigenbasis of the Hamiltonian where interaction terms between the local parts have been taken out. For example, in the Heisenberg model, the two-local measurement basis is given as the eigenbasis of the Hamiltonian

$$\hat{H}_2 = \sum_{i=1,3,5,7,9} (\hat{\sigma}_i^x \hat{\sigma}_{i+1}^x + \hat{\sigma}_i^y \hat{\sigma}_{i+1}^y + \hat{\sigma}_i^z \hat{\sigma}_{i+1}^z) + \sum_{i=1}^{10} h_i \hat{\sigma}_i^z. \quad (22)$$

This method ensures that for the full system ($k = L$), the measurement basis is the same as the eigenbasis of the observable that we optimize for. See Supplemental Material for details.

Upper bound on energy probabilities. First, we prove an upper bound on the energy probability,

$$p_E \leq \left(\sum_i \sqrt{p_i} \sqrt{\langle E | \hat{\Pi}_i | E \rangle} \right)^2, \quad (23)$$

where the right-hand side defines a_E . This is the second half of Eq. (18).

Proof. We express the spectral decomposition of the density matrix as $\hat{\rho} = \sum_m \lambda_m |\psi_m\rangle\langle\psi_m|$, where λ_m are its eigenvalues corresponding to eigenvectors $|\psi_m\rangle$. We find that $p_i = \text{tr}[\hat{\Pi}_i \hat{\rho}]$ translates to $p_i = \sum_m \lambda_m \langle\psi_m|\hat{\Pi}_i|\psi_m\rangle$. A series of inequalities follows:

$$\begin{aligned}
p_E &= \langle E | \hat{\rho} | E \rangle = \sum_m \lambda_m |\langle E | \psi_m \rangle|^2 = \sum_m \lambda_m \left| \sum_i \langle E | \hat{\Pi}_i | \psi_m \rangle \right|^2 \\
&\leq \sum_m \lambda_m \left(\sum_i |\langle E | \hat{\Pi}_i | \psi_m \rangle| \right)^2 \\
&= \sum_m \lambda_m \left(\sum_i \left| \langle E | \sqrt{\hat{\Pi}_i^\dagger} \sqrt{\hat{\Pi}_i} | \psi_m \rangle \right| \right)^2 \\
&\leq \sum_m \lambda_m \left(\sum_i \sqrt{\langle E | \hat{\Pi}_i | E \rangle \langle \psi_m | \hat{\Pi}_i | \psi_m \rangle} \right)^2 \\
&= \sum_m \lambda_m \|\mathbf{x}^m\|_{\frac{1}{2}} \\
&\leq \left\| \sum_m \lambda_m \mathbf{x}^m \right\|_{\frac{1}{2}} \\
&= \left(\sum_i \sqrt{\sum_m \lambda_m \langle E | \hat{\Pi}_i | E \rangle \langle \psi_m | \hat{\Pi}_i | \psi_m \rangle} \right)^2 \\
&= \left(\sum_i \sqrt{p_i} \sqrt{\langle E | \hat{\Pi}_i | E \rangle} \right)^2.
\end{aligned} \tag{24}$$

The first inequality is the triangle inequality, the second the Cauchy-Schwarz inequality, the third Jensen's theorem applied on $(p = \frac{1}{2})$ -seminorm

$$\|\mathbf{x}\|_{\frac{1}{2}} = \left(\sum_i \sqrt{x_i} \right)^2. \tag{25}$$

$\mathbf{x}^m = (x_1^m, x_2^m, \dots)$ is a vector of positive entries $x_i^m = \langle E | \hat{\Pi}_i | E \rangle \langle \psi_m | \hat{\Pi}_i | \psi_m \rangle \geq 0$. In order to apply Jensen's theorem, we need to first confirm that the $(p = \frac{1}{2})$ -seminorm is a concave function. It is concave when restricted on vectors with positive entries, $\|\cdot\|_{\frac{1}{2}} : \mathbb{R}_+^N \rightarrow \mathbb{R}_+$, which is indeed the case here. This follows from the reverse Minkowski inequality

$$\|\mathbf{x} + \mathbf{y}\|_p \geq \|\mathbf{x}\|_p + \|\mathbf{y}\|_p, \tag{26}$$

(where it is assumed $x_i \geq 0$, $y_i \geq 0$), which holds for all $(p < 1)$ -seminorms. Taking $0 \leq q \leq 1$, we have

$$\begin{aligned}
\|q\mathbf{x} + (1-q)\mathbf{y}\|_p &\geq \|q\mathbf{x}\|_p + \|(1-q)\mathbf{y}\|_p \\
&= q\|\mathbf{x}\|_p + (1-q)\|\mathbf{y}\|_p,
\end{aligned} \tag{27}$$

so $\|\cdot\|_{\frac{1}{2}}$ is indeed concave. \square

Lower bound on energy probabilities. Next we prove a lower bound on the energy probabilities,

$$p_E \geq \max \left\{ \sum_i p_i (x_i^E + \gamma_i y_i^E) - \left(\sum_i \sqrt{p_i y_i^E V_i} \right)^2, 0 \right\}. \tag{28}$$

where the right hand side defines b_E . This is the first half of Eq. (18), above which x_i^E , y_i^E , and V_i are defined. We drop superscripts E to keep the notation cleaner, i.e., we write $x_i \equiv x_i^E$ and $y_i \equiv y_i^E$.

Proof. It is clear that $p_E \geq 0$. We start by expressing p_E in a more convenient form to derive the first inequality.

$$\begin{aligned}
p_E &= \langle E | \hat{\rho} | E \rangle = \sum_m \lambda_m \left| \sum_i \langle E | \hat{\Pi}_i | \psi_m \rangle \right|^2 \\
&= \sum_m \lambda_m \left| \sum_{i,k} \gamma_i^k \langle E | i^k \rangle \langle i^k | \psi_m \rangle \right|^2 \\
&= \sum_{m,i,k} \lambda_m |\gamma_i^k \langle E | i^k \rangle \langle i^k | \psi_m \rangle|^2 \\
&\quad + \sum_{m,i \neq i', k, k'} \lambda_m \gamma_i^k \gamma_{i'}^{k'} \langle i'^{k'} | E \rangle \langle E | i^k \rangle \langle i^k | \psi_m \rangle \langle \psi_m | i'^{k'} \rangle \\
&\quad + \sum_{m,i,k \neq k'} \lambda_m \gamma_i^k \gamma_i^{k'} \langle i^{k'} | E \rangle \langle E | i^k \rangle \langle i^k | \psi_m \rangle \langle \psi_m | i^{k'} \rangle \\
&\geq \sum_{m,i,k} \lambda_m |\gamma_i^k \langle E | i^k \rangle \langle i^k | \psi_m \rangle|^2 + \sum_{m,i,k} \lambda_m |\gamma_i^k \langle i^k | \psi_m \rangle|^2 y_i - w \\
&\geq \sum_{m,i,k} \lambda_m \gamma_i^k |\langle i^k | \psi_m \rangle|^2 (x_i + \gamma_i y_i) - w \\
&= \sum_i p_i (x_i + \gamma_i y_i) - w.
\end{aligned} \tag{29}$$

The first inequality follows from the definition of absolute value and the second from definitions of x_i and γ_i . We defined

$$\begin{aligned}
w &= \sum_{m,i \neq i', k, k'} \lambda_m \gamma_i^k \gamma_{i'}^{k'} |\langle i'^{k'} | E \rangle \langle E | i^k \rangle \langle i^k | \psi_m \rangle \langle \psi_m | i'^{k'} \rangle| \\
&\quad + \sum_{m,i,k \neq k'} \lambda_m \gamma_i^k \gamma_i^{k'} |\langle i^{k'} | E \rangle \langle E | i^k \rangle \langle i^k | \psi_m \rangle \langle \psi_m | i^{k'} \rangle| \\
&\quad + \sum_{m,i,k} \lambda_m |\gamma_i^k \langle i^k | \psi_m \rangle|^2 y_i \\
&\leq \sum_{m,i,i',k,k'} \lambda_m \gamma_i^k \gamma_{i'}^{k'} |\langle i^k | \psi_m \rangle \langle \psi_m | i'^{k'} \rangle| \sqrt{y_i y_{i'}} \\
&= \sum_{i,i'} \sqrt{y_i y_{i'}} \sum_m \lambda_m \left(\sum_k \gamma_i^k |\langle i^k | \psi_m \rangle| \right) \left(\sum_{k'} \gamma_{i'}^{k'} |\langle i'^{k'} | \psi_m \rangle| \right) \\
&\leq \sum_{i,i'} \sqrt{y_i y_{i'}} \sum_m \lambda_m \left(\sqrt{\sum_k \gamma_i^k |\langle i^k | \psi_m \rangle|^2} \sqrt{\sum_k \gamma_i^k} \right) \\
&\quad \times \left(\sqrt{\sum_{k'} \gamma_{i'}^{k'} |\langle i'^{k'} | \psi_m \rangle|^2} \sqrt{\sum_{k'} \gamma_{i'}^{k'}} \right) \\
&= \sum_{i,i'} \sqrt{y_i y_{i'}} V_i V_{i'} \sum_m \lambda_m \|\vec{a}_i^m\|_2 \|\vec{a}_{i'}^{m'}\|_2 \\
&\leq \sum_{i,i'} \sqrt{y_i y_{i'}} V_i V_{i'} \sqrt{\sum_m \lambda_m \|\vec{a}_i^m\|_2^2} \sqrt{\sum_{m'} \lambda_{m'} \|\vec{a}_{i'}^{m'}\|_2^2} \\
&= \sum_{i,i'} \sqrt{p_i p_{i'} y_i y_{i'} V_i V_{i'}} \left(\sum_i \sqrt{p_i y_i V_i} \right)^2.
\end{aligned} \tag{30}$$

where $V_i = \sum_k \gamma_i^k$, $p_i = \sum_m \lambda_m \|\vec{a}_i^m\|_2^2$, $\vec{a}_i^m = (\sqrt{\gamma_i^1}|\langle i^1|\psi_m \rangle|, \sqrt{\gamma_i^2}|\langle i^2|\psi_m \rangle|, \dots)$, and $\|\cdot\|_2$ is the two-norm. The first inequality follows from the definition of y_i . We used the Cauchy-Schwarz inequality of type $|\sum_i a_i b_i| \leq \sqrt{\sum_i a_i^2} \sqrt{\sum_i b_i^2}$ in the second and the third inequality. Combining the two bounds, we obtain Eq. (28). \square

Proof of collective bounds. Finally, we prove

$$\sqrt{\mathbf{p}}^T \mathbf{A}_i \sqrt{\mathbf{p}} \leq p_i, \quad (31)$$

where $\sqrt{\mathbf{p}}_E = \sqrt{p_E}$ and $(\mathbf{A}_i)_{EE'} = (-1)^{1+\delta_{EE'}} |\langle E|\hat{\Pi}_i|E'\rangle|$. Expanding this gives $\sum_{E,E'} \sqrt{p_E} (\mathbf{A}_i)_{EE'} \sqrt{p_{E'}} \leq p_i$.

Proof.

$$\begin{aligned} p_i &= \text{tr}[\hat{\Pi}_i \hat{\rho}] = \sum_{E,E'} \text{tr}[|E\rangle\langle E|\hat{\Pi}_i|E'\rangle\langle E'|\hat{\rho}|E\rangle] \\ &= \sum_{E,E'} \langle E|\hat{\Pi}_i|E'\rangle\langle E'|\hat{\rho}|E\rangle \\ &= \sum_E \langle E|\hat{\Pi}_i|E\rangle p_E + \sum_{E \neq E'} \langle E|\hat{\Pi}_i|E'\rangle\langle E'|\hat{\rho}|E\rangle \\ &\geq \sum_E \langle E|\hat{\Pi}_i|E\rangle p_E - \sum_{E \neq E'} |\langle E|\hat{\Pi}_i|E'\rangle| |\langle E'|\hat{\rho}|E\rangle| \quad (32) \\ &\geq \sum_E \langle E|\hat{\Pi}_i|E\rangle p_E - \sum_{E \neq E'} |\langle E|\hat{\Pi}_i|E'\rangle| \sqrt{p_E p_{E'}} \\ &= 2 \sum_E \langle E|\hat{\Pi}_i|E\rangle p_E - \sum_{E,E'} |\langle E|\hat{\Pi}_i|E'\rangle| \sqrt{p_E p_{E'}} \\ &= \sum_{E,E'} \sqrt{p_E} (\mathbf{A}_i)_{EE'} \sqrt{p_{E'}}, \end{aligned}$$

where $p_E = \langle E|\hat{\rho}|E\rangle$. For the last inequality, we have used the fact that $\hat{\rho}$ is positive semi-definite, and therefore according to Sylvester's criterion for positive semi-definite matrices [99], which says that all submatrices

must have a non-negative determinant (i.e., all the principal minors are non-negative). For 2 by 2 submatrices this means

$$\langle E|\hat{\rho}|E\rangle\langle E'|\hat{\rho}|E'\rangle - \langle E|\hat{\rho}|E'\rangle\langle E'|\hat{\rho}|E\rangle \geq 0, \quad (33)$$

and thus $|\langle E'|\hat{\rho}|E\rangle|^2 \leq p_E p_{E'}$. The second inequality, $\sqrt{\mathbf{p}}^T \mathbf{B}_i \sqrt{\mathbf{p}} \geq p_i$, is proved analogously. \square

Acknowledgments. We thank Felix C. Binder for the collaboration on a related project during which some of the ideas for this paper started to surface. We thank Dung Xuan Nguyen, Sungjong Woo, and Siranuysh Badalyan for their comments and discussions. We acknowledge the support from the Institute for Basic Science in Korea (IBS-R024-D1).

Author Contributions. D.Š. Conceptualization, theory, bounds and their proofs in particular, writing, visualization of figures, development of the ground state optimized and the observable optimized (type 1) methods, and creating a single qubit example in the Supplemental Material. D.R. Development of the software for generating numerical experiments of Heisenberg, XY, PXP, and Ising models and producing the data, editing, and development of the observable optimized (type 2) method. Both authors contributed to the style of the paper and cross-contributed to the main roles of the other through frequent discussions.

Competing interests. Authors declare no competing financial or non-financial interests.

Data availability. Data is available from the corresponding authors upon reasonable request.

Code availability. The code used to generate data for this paper are available from the corresponding authors upon reasonable request.

[1] L. D'Alessio, Y. Kafri, A. Polkovnikov, and M. Rigol, *Advances in Physics* **65**, 239 (2016), arXiv:1509.06411 [cond-mat.stat-mech].

[2] J. M. Deutsch, *Reports on Progress in Physics* **81**, 082001 (2018), arXiv:1805.01616 [quant-ph].

[3] M. Vojta, *Reports on Progress in Physics* **66**, 2069 (2003).

[4] Z.-Y. Sun, Y.-Y. Wu, J. Xu, H.-L. Huang, B.-F. Zhan, B. Wang, and C.-B. Duan, *Phys. Rev. A* **89**, 022101 (2014).

[5] T. Tian, H.-X. Yang, L.-Y. Qiu, H.-Y. Liang, Y.-B. Yang, Y. Xu, and L.-M. Duan, *Phys. Rev. Lett.* **124**, 043001 (2020).

[6] H. P. Yuen and V. W. S. Chan, *Opt. Lett.* **8**, 177 (1983).

[7] T. Tyc and B. C. Sanders, *Journal of Physics A: Mathematical and General* **37**, 7341 (2004).

[8] Y. Shaked, Y. Michael, R. Z. Vered, L. Bello, M. Rosenbluh, and A. Pe'er, *Nature Communications* **9**, 609 (2018).

[9] F. Raffaelli, G. Ferranti, D. H. Mahler, P. Sibson, J. E. Kennard, A. Santamato, G. Sinclair, D. Bonneau, M. G. Thompson, and J. C. F. Matthews, *Quantum Science and Technology* **3**, 025003 (2018).

[10] D. Noll, D. Nishimura, and A. Macovski, *IEEE Transactions on Medical Imaging* **10**, 154 (1991).

[11] P. Voss, *Optical homodyne detection and applications in quantum cryptography*, Ph.D. thesis, TELECOM Paris-Tech (2009).

[12] L. Davidovich, *Rev. Mod. Phys.* **68**, 127 (1996).

[13] Y. Takeno, M. Yukawa, H. Yonezawa, and A. Furusawa, *Opt. Express* **15**, 4321 (2007).

[14] B. J. Lawrie, P. D. Lett, A. M. Marino, and R. C. Pooser, *ACS Photonics* **6**, 1307 (2019), <https://doi.org/10.1021/acsphotonics.9b00250>.

[15] W. Heisenberg, in *Original Scientific Papers Wissenschaftliche Originalarbeiten* (Springer, 1985) pp. 478–504.

[16] H. P. Robertson, *Phys. Rev.* **34**, 163 (1929).

[17] P. Busch, T. Heinonen, and P. Lahti, *Physics Reports* **452**, 155 (2007).

[18] A. S. Wightman, *Phys. Rev.* **101**, 860 (1956).

[19] M. Srednicki, *Quantum field theory* (Cambridge University Press, 2007).

[20] C. Bunge, J. Barrientos, and A. Bunge, *Atomic Data and Nuclear Data Tables* **53**, 113 (1993).

[21] A. N. Ikot, U. S. Okorie, R. Sever, and G. J. Rampho, *European Physical Journal Plus* **134**, 386 (2019).

[22] J. M. Deutsch, *New Journal of Physics* **12**, 075021 (2010).

[23] R. H. Swendsen, arXiv e-prints , arXiv:1508.01323 (2015), arXiv:1508.01323 [cond-mat.stat-mech].

[24] L. F. Santos, A. Polkovnikov, and M. Rigol, *Phys. Rev. Lett.* **107**, 040601 (2011).

[25] D. Šafránek, A. Aguirre, J. Schindler, and J. M. Deutsch, *Foundations of Physics* **51**, 101 (2021), arXiv:2008.04409 [quant-ph].

[26] K. V. Hovhannisyan and L. A. Correa, *Phys. Rev. B* **98**, 045101 (2018).

[27] V. Mukherjee, A. Zwick, A. Ghosh, X. Chen, and G. Kurizki, *Communications Physics* **2**, 1 (2019).

[28] M. F. B. Cenni, L. Lami, A. Acin, and M. Mehboodi, arXiv e-prints , arXiv:2110.02098 (2021), arXiv:2110.02098 [quant-ph].

[29] A. Engel and R. Nolte, *Europhysics Letters* **79**, 10003 (2007).

[30] S. Alipour, F. Benatti, F. Bakhshinezad, M. Afsary, S. Marcantoni, and A. T. Rezakhani, *Scientific Reports* **6**, 35568 (2016), arXiv:1606.08869 [quant-ph].

[31] R. Modak and M. Rigol, *Phys. Rev. E* **95**, 062145 (2017).

[32] J. Goold, F. Plastina, A. Gambassi, and A. Silva, “The role of quantum work statistics in many-body physics,” in *Thermodynamics in the Quantum Regime: Fundamental Aspects and New Directions*, edited by F. Binder, L. A. Correa, C. Gogolin, J. Anders, and G. Adesso (Springer International Publishing, Cham, 2018) pp. 317–336.

[33] G. De Chiara, P. Solinas, F. Cerisola, and A. J. Roncaglia, “Ancilla-assisted measurement of quantum work,” in *Thermodynamics in the Quantum Regime: Fundamental Aspects and New Directions*, edited by F. Binder, L. A. Correa, C. Gogolin, J. Anders, and G. Adesso (Springer International Publishing, Cham, 2018) pp. 337–362.

[34] A. D. Varizi, A. P. Vieira, C. Cormick, R. C. Drumond, and G. T. Landi, *Phys. Rev. Research* **2**, 033279 (2020).

[35] A. E. Allahverdyan, R. Balian, and T. M. Nieuwenhuizen, *Europhysics Letters (EPL)* **67**, 565 (2004).

[36] R. Alicki and M. Fannes, *Phys. Rev. E* **87**, 042123 (2013).

[37] D. Šafránek, D. Rosa, and F. Binder, arXiv e-prints , arXiv:2209.11076 (2022), arXiv:2209.11076 [quant-ph].

[38] M. G. A. Paris, arXiv e-prints , arXiv:0804.2981 (2008), arXiv:0804.2981 [quant-ph].

[39] L. A. Correa, M. Mehboodi, G. Adesso, and A. Sanpera, *Phys. Rev. Lett.* **114**, 220405 (2015), arXiv:1411.2437 [quant-ph].

[40] L. Mandelstam and I. Tamm, “The uncertainty relation between energy and time in non-relativistic quantum mechanics,” in *Selected Papers*, edited by B. M. Bologtovskii, V. Y. Frenkel, and R. Peierls (Springer Berlin Heidelberg, Berlin, Heidelberg, 1991) pp. 115–123.

[41] N. Margolus and L. B. Levitin, *Physica D: Nonlinear Phenomena* **120**, 188 (1998), proceedings of the Fourth Workshop on Physics and Consumption.

[42] S. Deffner and S. Campbell, *Journal of Physics A Mathematical General* **50**, 453001 (2017), arXiv:1705.08023 [quant-ph].

[43] L. Villa and G. De Chiara, arXiv e-prints , arXiv:1704.01583 (2017), arXiv:1704.01583 [quant-ph].

[44] J. L. Jiménez, S. P. G. Crone, E. Fogh, M. E. Zayed, R. Lortz, E. Pomjakushina, K. Conder, A. M. Läuchli, L. Weber, S. Wessel, A. Honecker, B. Normand, C. Rüegg, P. Corboz, H. M. Rønnow, and F. Mila, *Nature (London)* **592**, 370 (2021).

[45] M. A. Nielsen and I. Chuang, “Quantum computation and quantum information,” (American Association of Physics Teachers, 2002) Chap. 9.3.

[46] D. M. Reich, G. Gualdi, and C. P. Koch, *Phys. Rev. Lett.* **111**, 200401 (2013).

[47] R. Harper and S. T. Flammia, *Quantum Science and Technology* **2**, 015008 (2017), arXiv:1608.02943 [quant-ph].

[48] W. Huang, C. H. Yang, K. W. Chan, T. Tanttu, B. Hensen, R. C. C. Leon, M. A. Fogarty, J. C. C. Hwang, F. E. Hudson, K. M. Itoh, A. Morello, A. Laucht, and A. S. Dzurak, *Nature (London)* **569**, 532 (2019), arXiv:1805.05027 [cond-mat.mes-hall].

[49] J. Combes and A. P. Lund, arXiv e-prints , arXiv:2207.10210 (2022), arXiv:2207.10210 [quant-ph].

[50] D. S. Hochbaum, *Annals of Operations Research* **153**, 257 (2007).

[51] M. A. Luersen and R. Le Riche, *Computers & Structures* **82**, 2251 (2004), computational Structures Technology.

[52] W. Price, *Journal of optimization theory and applications* **40**, 333 (1983).

[53] R. Storn, in *Proceedings of north american fuzzy information processing* (Ieee, 1996) pp. 519–523.

[54] S. Sivanandam and S. Deepa, in *Introduction to genetic algorithms* (Springer, 2008) pp. 165–209.

[55] D. Bertsimas and J. Tsitsiklis, *Statistical science* **8**, 10 (1993).

[56] A. Das and B. K. Chakrabarti, *Quantum annealing and related optimization methods*, Vol. 679 (Springer Science & Business Media, 2005).

[57] M. J. Powell, *Acta numerica* **7**, 287 (1998).

[58] J. von Neumann, *European Physical Journal H* **35**, 201 (2010).

[59] D. Šafránek, J. M. Deutsch, and A. Aguirre, *Phys. Rev. A* **99**, 010101 (2019), arXiv:1707.09722 [quant-ph].

[60] D. Šafránek, J. M. Deutsch, and A. Aguirre, *Phys. Rev. A* **99**, 012103 (2019), arXiv:1803.00665 [quant-ph].

[61] P. Strasberg and A. Winter, *PRX Quantum* **2**, 030202 (2021), arXiv:2002.08817 [quant-ph].

[62] F. Buscemi, J. Schindler, and D. Šafránek, arXiv:2209.03803 (2022), 10.48550/arXiv.2209.03803.

[63] D. Šafránek and J. Thingna, arXiv e-prints , arXiv:2007.07246 (2020), arXiv:2007.07246 [quant-ph].

[64] G. Usaj, H. M. Pastawski, and P. R. Levine, *Molecular Physics* **95**, 1229 (1998), <https://doi.org/10.1080/00268979809483253>.

[65] C. Sánchez, P. Levstein, L. Buljubasich, H. Pastawski, and A. Chattah, *Philosophical Transactions of the Royal Society A: Mathematical, Physical and Engineering Sciences* **374**, 20150155 (2016).

[66] H. M. Pastawski, P. R. Levstein, and G. Usaj, *Phys. Rev. Lett.* **75**, 4310 (1995).

[67] P. R. Levstein, A. K. Chattah, H. M. Pastawski, J. Raya, and J. Hirschinger, *The Journal of Chemical Physics* **121**, 7313 (2004), <https://doi.org/10.1063/1.1792575>.

[68] B. Rauer, S. Erne, T. Schwegler, F. Cataldini, M. Tajik, and J. Schmiedmayer, *Science* **360**, 307 (2018), <https://www.science.org/doi/pdf/10.1126/science.aaan7938>.

[69] D. A. Abanin, E. Altman, I. Bloch, and M. Serbyn, *Rev. Mod. Phys.* **91**, 021001 (2019).

[70] D. Porras and J. I. Cirac, *Phys. Rev. Lett.* **92**, 207901 (2004).

[71] A. Pal and D. A. Huse, *Phys. Rev. B* **82**, 174411 (2010).

[72] D. J. Luitz, N. Laflorencie, and F. Alet, *Phys. Rev. B* **91**, 081103 (2015).

[73] J. Smith, A. Lee, P. Richerme, B. Neyenhuis, P. W. Hess, P. Hauke, M. Heyl, D. A. Huse, and C. Monroe, *Nature Physics* **12**, 907 (2016), [arXiv:1508.07026 \[quant-ph\]](https://arxiv.org/abs/1508.07026).

[74] P. Jurcevic, H. Shen, P. Hauke, C. Maier, T. Brydges, C. Hempel, B. P. Lanyon, M. Heyl, R. Blatt, and C. F. Roos, *Phys. Rev. Lett.* **119**, 080501 (2017).

[75] J. Zhang, G. Pagano, P. W. Hess, A. Kyprianidis, P. Becker, H. Kaplan, A. V. Gorshkov, Z. X. Gong, and C. Monroe, *Nature (London)* **551**, 601 (2017), [arXiv:1708.01044 \[quant-ph\]](https://arxiv.org/abs/1708.01044).

[76] N. S. Bingham, S. Rooke, J. Park, A. Simon, W. Zhu, X. Zhang, J. Batley, J. D. Watts, C. Leighton, K. A. Dahmen, and P. Schiffer, *Phys. Rev. Lett.* **127**, 207203 (2021).

[77] B. Lanyon, C. Maier, M. Holzäpfel, T. Baumgratz, C. Hempel, P. Jurcevic, I. Dhand, A. Buyskikh, A. Dalley, M. Cramer, *et al.*, *Nature Physics* **13**, 1158 (2017).

[78] N. Friis, O. Marty, C. Maier, C. Hempel, M. Holzäpfel, P. Jurcevic, M. B. Plenio, M. Huber, C. Roos, R. Blatt, and B. Lanyon, *Phys. Rev. X* **8**, 021012 (2018).

[79] T. Brydges, A. Elben, P. Jurcevic, B. Vermersch, C. Maier, B. P. Lanyon, P. Zoller, R. Blatt, and C. F. Roos, *Science* **364**, 260 (2019).

[80] C. Maier, T. Brydges, P. Jurcevic, N. Trautmann, C. Hempel, B. P. Lanyon, P. Hauke, R. Blatt, and C. F. Roos, *Phys. Rev. Lett.* **122**, 050501 (2019).

[81] H. Bernien, S. Schwartz, A. Keesling, H. Levine, A. Omran, H. Pichler, S. Choi, A. S. Zibrov, M. Endres, M. Greiner, V. Vuletić, and M. D. Lukin, *Nature (London)* **551**, 579 (2017), [arXiv:1707.04344 \[quant-ph\]](https://arxiv.org/abs/1707.04344).

[82] C. J. Turner, A. A. Michailidis, D. A. Abanin, M. Serbyn, and Z. Papić, *Nature Physics* **14**, 745 (2018).

[83] G.-X. Su, H. Sun, A. Hudomal, J.-Y. Desaules, Z.-Y. Zhou, B. Yang, J. C. Halimeh, Z.-S. Yuan, Z. Papić, and J.-W. Pan, arXiv e-prints, arXiv:2201.00821 (2022), [arXiv:2201.00821 \[cond-mat.quant-gas\]](https://arxiv.org/abs/2201.00821).

[84] H. Bethe, *Zeitschrift für Physik* **71**, 205 (1931).

[85] M. J. Powell, in *Advances in optimization and numerical analysis* (Springer, 1994) pp. 51–67.

[86] H.-Y. Huang, R. Kueng, and J. Preskill, *Nature Physics* **16**, 1050 (2020), [arXiv:2002.08953 \[quant-ph\]](https://arxiv.org/abs/2002.08953).

[87] M. Benedetti, J. Realpe-Gómez, R. Biswas, and A. Perdomo-Ortiz, *Phys. Rev. A* **94**, 022308 (2016).

[88] M. Pino and J. J. García-Ripoll, *Phys. Rev. A* **101**, 032324 (2020).

[89] P. Hauke, H. G. Katzgraber, W. Lechner, H. Nishimori, and W. D. Oliver, *Reports on Progress in Physics* **83**, 054401 (2020), [arXiv:1903.06559 \[quant-ph\]](https://arxiv.org/abs/1903.06559).

[90] T. Imoto, Y. Seki, Y. Matsuzaki, and S. Kawabata, arXiv e-prints, arXiv:2102.05323 (2021), [arXiv:2102.05323 \[quant-ph\]](https://arxiv.org/abs/2102.05323).

[91] N. Mohseni, M. Naroziak, A. N. Pyrkov, V. Ivanikov, J. P. Dowling, and T. Byrnes, arXiv e-prints, arXiv:1909.09947 (2019), [arXiv:1909.09947 \[quant-ph\]](https://arxiv.org/abs/1909.09947).

[92] J. Eisert, M. Cramer, and M. B. Plenio, *Rev. Mod. Phys.* **82**, 277 (2010).

[93] M. B. Hastings, *Journal of Statistical Mechanics: Theory and Experiment* **2007**, P08024 (2007).

[94] B. M. Terhal, *Physics Letters A* **271**, 319 (2000), [arXiv:quant-ph/9911057 \[quant-ph\]](https://arxiv.org/abs/quant-ph/9911057).

[95] M. Barbieri, F. De Martini, G. Di Nepi, P. Mataloni, G. M. D’Ariano, and C. Macchiavello, *Phys. Rev. Lett.* **91**, 227901 (2003).

[96] M. Lewenstein, B. Kraus, J. I. Cirac, and P. Horodecki, *Phys. Rev. A* **62**, 052310 (2000).

[97] R. Orús, *Annals of Physics* **349**, 117 (2014).

[98] J. Schindler, D. Šafránek, and A. Aguirre, *Phys. Rev. A* **102**, 052407 (2020).

[99] K. Swamy, *IEEE Transactions on Automatic Control* **18**, 306 (1973).

[100] V. Khemani, M. Hermele, and R. Nandkishore, *Phys. Rev. B* **101**, 174204 (2020).

[101] M. Serbyn, D. A. Abanin, and Z. Papić, *Nature Physics* **17**, 675 (2021).

[102] A. Chandran, T. Iadecola, V. Khemani, and R. Moessner, “Quantum many-body scars: A quasiparticle perspective,” (2022).

SUPPLEMENTAL MATERIAL

In this Supplemental Material, we provide several examples, derivations, and numerical experiments. It contains: Sec. I: Example in which the bound on the collection of energy probabilities provides a much better estimate of the mean energy value. Sec. II: Derivation of the analytic bound on the mean energy. Sec. III: Introduction of quality factors — two measures of performance. Sec. IV: Simple example of the mean energy estimation of a qubit. Sec. V: Estimation of the mean energy in experimentally relevant models: Heisenberg, Ising, XY, and PXP models.

I. POWERFUL IMPROVEMENT FROM COLLECTIVE BOUNDS

Here we show an example in which the collective bounds

$$\sqrt{\mathbf{p}}^T \mathbf{A}_i \sqrt{\mathbf{p}} \leq p_i^{\min} \leq p_i^{\max} \leq \sqrt{\mathbf{p}}^T \mathbf{B}_i \sqrt{\mathbf{p}}, \quad (34)$$

(Eq. (7) in the main text) where

$$p_i^{\min} = \min_{t \in [0, T]} p_i(t), \quad p_i^{\max} = \max_{t \in [0, T]} p_i(t), \quad (35)$$

provide a considerable improvement in the estimation of energy probabilities in comparison with using just the

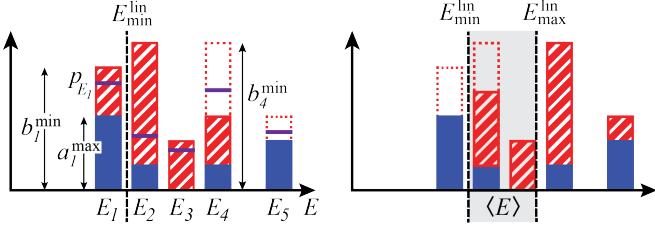


FIG. 4. The lower bound (left) is found by filling the minimal probability of each energy given by a_l^{\max} (blue solid), and topping it up to the maximum b_l^{\min} (red striped), from the lowest to the highest energy, until the probabilities sum up to one. The upper bound (right) is obtained by the same method, but going from the highest to the lowest energy. The mean energy $\langle E \rangle$ lies somewhere in the shaded region.

linear bound

$$a_E^{\max} \leq p_E \leq b_E^{\min}. \quad (36)$$

(Eq. (3) in the main text.)

Consider a coarse-grained energy measurement given by the coarse-grained energy projectors

$$\hat{P}_{\tilde{E}} = \sum_{E \in [\tilde{E}, \tilde{E} + \Delta E]} |E\rangle\langle E|. \quad (37)$$

ΔE denotes the resolution in measuring energy. Then $\mathbf{A}_i = \mathbf{B}_i$ are diagonal and the inequalities yield

$$p_{\tilde{E}} = p_{\tilde{E}}^{\max} = p_{\tilde{E}}^{\min} = \sum_{E \in [\tilde{E}, \tilde{E} + \Delta E]} p_E. \quad (38)$$

This upper bounds the sum of energy probabilities, making the determination of the mean energy much more precise. This is a stark difference with Eq. (36), which yields much less restrictive $p_E \leq p_{\tilde{E}}$ for each $E \in [\tilde{E}, \tilde{E} + \Delta E]$.

II. DERIVATION OF THE ANALYTIC BOUND ON THE MEAN ENERGY

Here we derive the recurrence formula for computation of the lower bound upper values of the bound

$$E_{\min}^{\text{lin}} \leq \langle E \rangle \leq E_{\max}^{\text{lin}}. \quad (39)$$

We do this with the lower value, E_{\min}^{lin} , and the formula for the upper value with follow analogously.

The lower bound is given by

$$E_{\min}^{\text{lin}} = \sum_{l=1}^N E_l u_l. \quad (40)$$

(Eq. (11) in the main text), where u_l follow a recurrence relation that we derive next. We simplified the lower indices as $l \equiv E_l$.

The idea behind the recurrence relation is described in Fig. 4, which corresponds to Fig. 1 in the main text. Having bounds

$$a_l^{\max} \equiv a_{E_l}^{\max} \leq p_{E_l} \leq b_{E_l}^{\min} \equiv b_l^{\min}, \quad (41)$$

(Eq. (3) in the main text) we find the lower bound on the mean energy by by filling the minimal probability of each energy given by a_l^{\max} , and topping it up up to the maximum b_l^{\min} , from the lowest to the highest energy, until the probabilities sum up to one.

What does this mean mathematically? Let us think of a “bottle” of probabilities with the full volume equal to one, $V = 1$. We start with all u_l initialized at zero. We pour the minimal required amount given by $a_l^{\max} \leq p_E$ into each probability u_l . After this, we have

$$\begin{aligned} u_1 &= a_1^{\max} \\ u_2 &= a_2^{\max} \\ &\dots \\ u_N &= a_N^{\max} \end{aligned} \quad (42)$$

and the remaining volume in the bottle is $V = 1 - \sum_{l=1}^N a_l^{\max}$. Now we start topping each u_l up to its maximum value, from the lowest to the highest energy eigenvalue, until we run out of the probability in the bottle. For $l = 1$, the two cases can occur: either there is enough probability in the bottle to fill u_l up to its maximum allowed value b_1^{\min} , or not. Mathematically, this topping up is expressed as

$$u_1 = a_1^{\max} + \min \left\{ b_1^{\min} - a_1^{\max}, 1 - \sum_{l=1}^N a_l^{\max} \right\}. \quad (43)$$

The a_1^{\max} can be subtracted, which gives

$$u_1 = \min \left\{ b_1^{\min}, 1 - \sum_{l=2}^N a_l^{\max} \right\}. \quad (44)$$

The remaining volume in the bottle is $V = 1 - u_1 - \sum_{l=2}^N a_l^{\max}$.

Next, we top up the second probability, which gives

$$\begin{aligned} u_2 &= a_2^{\max} + \min \left\{ b_2^{\min} - a_2^{\max}, 1 - u_1 - \sum_{l=2}^N a_l^{\max} \right\} \\ &= \min \left\{ b_2^{\min}, 1 - u_1 - \sum_{l=3}^N a_l^{\max} \right\}. \end{aligned} \quad (45)$$

The remaining volume is $V = 1 - \sum_{l=1}^2 u_l - \sum_{l=3}^N a_l^{\max}$. We continue up to the maximal index N , deriving the full recursive relation, Eq. (12) in the main text.

The recursive relation for E_{\max}^{lin} is derived analogously.

III. QUALITY FACTORS

We can employ two quality factors to assess the performance of method four bounding the mean energy: the

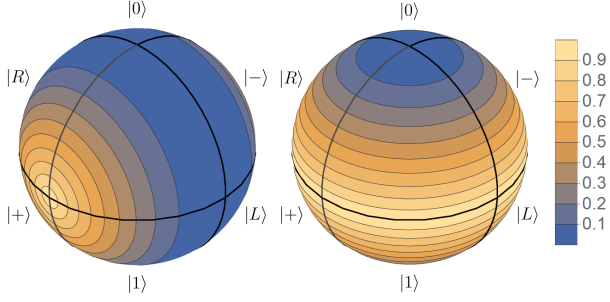


FIG. 5. Illustration of the performance when estimating energy by local Pauli- x measurements in a simple qubit example. We show the quality Q_1 factor—percentage of excluded energies, when estimating energy given by the Hamiltonian $\hat{H} = \hat{\sigma}_z$ by measuring in the $\hat{\sigma}_x$ basis, for different initial states on the Bloch sphere. Left panel: Quality factor of the initial state. Value $Q_1 = 1$ (light orange; which happens for state $|\psi\rangle = |+\rangle$) corresponds to perfect identification of the energy, while value $Q_1 = 0$ (dark blue; which happens for state $|\psi\rangle = |0\rangle$) corresponds to failure in identifying the energy. Right panel: the quality factor over initial states if we allow time evolution of the state with the Hamiltonian, and measure at different times $t \in [0, \pi/2]$ to build up statistics of outcomes at each time of this interval. The Hamiltonian revolves the state around the z -axis, so during the time evolution, the state picks up the best quality factor at that latitude from the figure on the left.

first,

$$Q_1 = \left(1 - \frac{E_{\max} - E_{\min}}{E_N - E_1}\right) \times 100\%, \quad (46)$$

which measures the range of excluded energy, and the second,

$$Q_2 = \left(1 - \frac{N_{[E_{\min}, E_{\max}]}}{N}\right) \times 100\%, \quad (47)$$

which measures the percentage of “excluded” energy eigenstates. $N_{[E_{\min}, E_{\max}]}$ denotes the number of energy eigenstates with energy between E_{\min} and E_{\max} , and N is the dimension of the Hilbert space.

IV. SIMPLE EXAMPLE

Consider a Hamiltonian given by the Pauli- z Matrix,

$$\hat{H} = \hat{\sigma}_z = \begin{pmatrix} 1 & 0 \\ 0 & -1 \end{pmatrix}, \quad (48)$$

which has energy eigenvalues $E_0 = -1$ and $E_1 = 1$, corresponding to eigenstates $|0\rangle$ and $|1\rangle$, respectively. The task is to estimate the energy of a general pure qubit state,

$$|\psi\rangle = \cos \frac{\theta}{2} |0\rangle + e^{i\phi} \sin \frac{\theta}{2} |1\rangle, \quad (49)$$

where $0 \leq \theta \leq \pi$ and $0 \leq \phi \leq 2\pi$.

We consider two different two-outcome measurements to estimate energy. We will use the combined bound for the energy probabilities,

$$\left| p_E - \sum_i p_i |\langle E | i \rangle|^2 \right| \leq b_E - \sum_i p_i |\langle E | i \rangle|^2, \quad (50)$$

where $b_E = (\sum_i \sqrt{p_i} |\langle E | i \rangle|)^2$, which is Eq. (1) in the main text.

First, consider measuring in the z -basis, i.e., measuring in the eigenbasis of operator $\hat{M} = \hat{\sigma}_z$. This defines the measurement $\mathcal{C} = \{|0\rangle\langle 0|, |1\rangle\langle 1|\}$. Because the measurement basis is the same as the eigenbasis of the Hamiltonian, we are measuring the energy directly so we expect the exact result. From the bound above we have

$$\begin{aligned} |p_{E_0} - p_0| &\leq 0, \\ |p_{E_1} - p_1| &\leq 0, \end{aligned} \quad (51)$$

independent of the initial state $|\psi\rangle$. Clearly, $p_{E_0} = p_0$, $p_{E_1} = p_1$, and $E_{\min}^{\text{lin}} = \langle E \rangle = E_{\max}^{\text{lin}}$, as expected.

Second, consider measuring in the x -basis, i.e., measuring in the eigenbasis of operator $\hat{M} = \hat{\sigma}_x$. This defines $\mathcal{C} = \{|+\rangle\langle +|, |-\rangle\langle -|\}$. We have

$$\begin{aligned} |p_{E_0} - \frac{1}{2}| &\leq \frac{1}{2}((\sqrt{p_+} + \sqrt{p_-})^2 - 1), \\ |p_{E_1} - \frac{1}{2}| &\leq \frac{1}{2}((\sqrt{p_+} + \sqrt{p_-})^2 - 1). \end{aligned} \quad (52)$$

This means that if the state is aligned with the x axis, for example, $p_+ = 1$, then $p_{E_0} = p_{E_1} = \frac{1}{2}$ and we can determine the energy exactly as $\langle E \rangle = 0$. On the contrary, if the state is aligned with the z -axis, implying $p_+ = p_- = \frac{1}{2}$, then $|p_{E_0} - \frac{1}{2}| \leq \frac{1}{2}$ and $|p_{E_1} - \frac{1}{2}| \leq \frac{1}{2}$ which we can rewrite as $0 \leq p_{E_0} \leq 1$ and $0 \leq p_{E_1} \leq 1$. Thus we obtain a trivial bound,

$$-1 = E_{\max}^{\text{lin}} \leq \langle E \rangle \leq E_{\max}^{\text{lin}} = 1. \quad (53)$$

Generally, we have

$$p_+ = \frac{1}{2}(1 + \cos \phi \sin \theta), \quad p_- = \frac{1}{2}(1 - \cos \phi \sin \theta). \quad (54)$$

which gives

$$\begin{aligned} |p_{E_0} - \frac{1}{2}| &\leq \frac{1}{2}\sqrt{1 - \cos^2 \phi \sin^2 \theta}, \\ |p_{E_1} - \frac{1}{2}| &\leq \frac{1}{2}\sqrt{1 - \cos^2 \phi \sin^2 \theta}. \end{aligned} \quad (55)$$

This yields

$$-\sqrt{1 - \cos^2 \phi \sin^2 \theta} = E_{\max}^{\text{lin}} \leq \langle E \rangle \leq E_{\max}^{\text{lin}} = \sqrt{1 - \cos^2 \phi \sin^2 \theta}. \quad (56)$$

We visualize the corresponding quality factor (the percentage of excluded energies, see Eq. (46))

$$Q_1 = 1 - \sqrt{1 - \cos^2 \phi \sin^2 \theta} \quad (57)$$

for this general case on the Bloch sphere in Fig. 5.

Next, we consider time evolution. We have

$$|\psi_t\rangle = e^{-i\hat{H}t}|\psi\rangle = \cos \frac{\theta}{2}|0\rangle + e^{i(\phi-2t)} \sin \frac{\theta}{2}|1\rangle. \quad (58)$$

Measuring $\hat{\sigma}_x$ at time t bounds the energy probabilities as

$$\begin{aligned} |p_{E_0} - \frac{1}{2}| &\leq \frac{1}{2}\sqrt{1 - \cos^2(\phi - 2t)\sin^2\theta}, \\ |p_{E_1} - \frac{1}{2}| &\leq \frac{1}{2}\sqrt{1 - \cos^2(\phi - 2t)\sin^2\theta}. \end{aligned} \quad (59)$$

If we measure at different times during $t \in [0, \pi/2]$, we manage to tighten these bounds and obtain

$$\begin{aligned} |p_{E_0} - \frac{1}{2}| &\leq \frac{1}{2}|\cos\theta|, \\ |p_{E_1} - \frac{1}{2}| &\leq \frac{1}{2}|\cos\theta|, \end{aligned} \quad (60)$$

which leads to bounds on energy

$$-|\cos\theta| = E_{\max}^{\text{lin}} \leq \langle E \rangle \leq E_{\max}^{\text{lin}} = |\cos\theta|. \quad (61)$$

The corresponding quality factor $Q_1 = 1 - |\cos\theta|$ is again plotted in Fig. 5.

V. ESTIMATION OF THE MEAN ENERGY IN EXPERIMENTALLY RELEVANT MODELS

Here we show the simulations for energy estimation using measurements in a local number basis and then using optimized k -local measurements. This is a continuation of numerical simulations shown in the main text, which contained a part of the results obtained for the Heisenberg model.

We simulate a number of models, including the Heisenberg model [70–72], which is a paradigmatic model to study for many-body localization, and then other several experimentally relevant models. These are the Ising model [73–76], known for its frequent use in quantum simulators and quantum annealers, the XY model [77–80], which is a type of non-integrable long-range model, and the PXP model [81–83], an archetypal model for many-body quantum scars.

The Hamiltonians and the corresponding parameters are given in Table I. The simulations of energy estimation using local particle number measurements and optimized k -local measurements are shown in Tables II and III.

The bulk of the explanation necessary to understand these numerical experiments are also shown in the main text. Below, we give details on the types of Hilbert space considered in our simulations, and we discuss methods that we designed for the optimization over the k -local measurements to estimate energy.

A. Hilbert space considered

In our simulations, we choose to work in a different type of Hilbert space for each model, depending on the

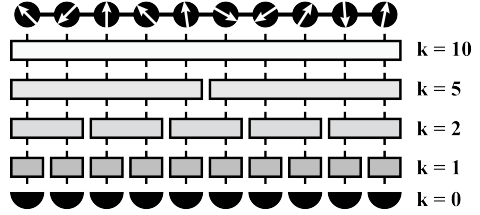


FIG. 6. Sketch of allowed operations. $k = 0$ corresponds to measuring in the local number basis. $k = 1$ allows for using single-site unitary operators leading to a general single-site measurement, $k = 2$ for two-site local operators, etc.

conservation laws, and to match the experimental setups, see Table I. In the Heisenberg and the XY models, the full Hilbert space splits into subspaces, each of them characterized by a definite value of the total spin along the z axes, i.e. $\hat{S}^z = \sum_i \hat{\sigma}_i^z$. We work in the largest subspace, which is characterized by the value $\hat{S}^z = 0$. This conservation is also the reason why the actual value of B in the XY model is irrelevant. For the Ising model, the total spin along the z axes is not conserved, only the *parity* of the total spin is conserved. In this case, we work on the parity even subspace, which is that containing the Néel state. For the PXP model, the situation is more intricate: the presence of the projector operators $(\hat{I} - \hat{\sigma}_i^z)$ in the Hamiltonian introduces a non-trivial local constraint [82]. As a consequence, the full Hilbert space shatters in a large number of different subspaces, dynamically disconnected and having various dimensions [100]. Inside each subspace, the dynamics is generically chaotic with the presence of *many-body scars* [82, 101, 102]. However, our goal in using this model was to study the effect of the Hilbert space shattering on the quality of the estimation of the energy. Therefore, we work in the full Hilbert space.

B. Methods for optimizing local measurements

We introduce three methods of analytical optimization for the k -local measurements. The sketch of k -local measurements is shown in Fig. 6, which corresponds to Fig 3 in the main text. k -local measurement consists of the application of a k -local unitary operator and then measuring in the computational basis.

1. Ground state-optimized measurements

First, we introduce a method that is k -local optimization for a specific state, in our case the ground state. This method is inspired by the Matrix Product State ansatz [97], and by the correspondence between observational and entanglement entropy [98].

The logic of the motivation goes as follows: low obser-

name	characteristics	conservation	Hamiltonian	parameters
Heisenberg (integrable, delocalized, (localized)	many-body localizing	total spin conserving	$\hat{H} = \sum_i (\hat{\sigma}_i^x \hat{\sigma}_{i+1}^x + \hat{\sigma}_i^y \hat{\sigma}_{i+1}^y + \hat{\sigma}_i^z \hat{\sigma}_{i+1}^z) + \sum_i h_i \hat{\sigma}_i^z$	$h_i \in [-W, W]$ drawn randomly ($W = 0, W = 0.5, W = 10$)
Ising (delocalized, localized)	gapped and many-body localizing	parity conserving	$\hat{H} = \sum_{i < j} J_{ij} \hat{\sigma}_i^x \hat{\sigma}_j^x + \frac{1}{2} \sum_i (B + h_i) \hat{\sigma}_i^z$	$J_0 = 1, \alpha = 1.13, B = 4,$ $h_i \in [-W, W]$ drawn randomly ($W = 0, W = 8$)
XY	gapped and long-range	total spin conserving	$\hat{H} = \sum_{i < j} J_{ij} (\hat{\sigma}_i^+ \hat{\sigma}_j^- + \hat{\sigma}_i^- \hat{\sigma}_j^+) + B \sum_i \hat{\sigma}_i^z$	$J_0 = 1, \alpha = 1.24, B = 0$
PXP	quantum scars	Hilbert space shattering	$\hat{H} = \frac{\Omega}{4} \sum_i (\hat{I} - \hat{\sigma}_i^z) \hat{\sigma}_{i+1}^x (\hat{I} - \hat{\sigma}_{i+2}^z)$	$\Omega = 1$
Sizes and Hilbert spaces considered in the numerical experiments				
Small systems			Large systems	
Heisenberg	6 sites, 3 particles	$D = 20$	10 sites, 5 particles	$D = 252$
Ising	6 sites, even parity subspace	$D = 32$	10 sites, even parity subspace	$D = 512$
XY	6 sites, 3 particles	$D = 20$	10 sites, 5 particles	$D = 252$
PXP	5 sites, full Hilbert space	$D = 32$	10 sites, full Hilbert space	$D = 1024$

TABLE I. Table of models used in our simulations and the Hilbert spaces considered with dimension D . $\hat{\sigma}_i^x$ denotes the Pauli-x matrix at site i , and similar with Pauli-y and Pauli-z matrices. $\hat{\sigma}_i^+$ and $\hat{\sigma}_i^-$ denote the spin creation and annihilation operators, respectively. In the Ising and XY models, we have a non-local interaction of form $J_{ij} = J_0/|i - j|^\alpha$. Parameters were taken to match those employed in experiments.

vational entropy means that the system state wandered into one of the small subspaces-macrostates given by the measurement [60, 63]. This means that we can estimate the maximal and the minimal value of the estimated observable in that subspace, which in turn translates into estimating these bounds for the system state itself. In other words, lower observational entropy means better estimates. According to Ref. [98], observational entropy minimized over local coarse-grainings leads to entanglement entropy, and the minimum is achieved when the local coarse-grainings are given by the Schmidt basis. This means that the measuring in the Schmidt basis will yield small observational entropy, and in turn better estimate of the mean value of observable. Thus, we need to find k -local measurements that reflect the Schmidt basis, and these are expected to perform well in the estimation.

We do this as follows: Assuming we have a chain of length L (for example, $L = 10$), and some divisor $k \leq 10$ (for example $k = 2$), we first divide the chain into two parts: one — system A_1 — of length k (i.e., sites (1, 2)) and the other — system B_1 — of length $L - k$ (i.e., sites (3, 4, 5, 6, 7, 8, 9, 10)). We define $\hat{\rho}_0$ as the ground state (or any other state that we want to optimize for). We compute the reduced density matrix

$$\hat{\rho}_{A_1} = \text{tr}_{B_1} \hat{\rho}_0, \quad (62)$$

and diagonalize it. The eigenbasis of the reduced density matrix is, by definition, the system A_1 -local part of the Schmidt basis. We denote this basis as $\{|\psi_{i_1}^{A_1}\rangle\}$.

Then we move onto the next k sites. We divide the system into A_2 (sites (3, 4)) and B_2 (sites (1, 2, 5, 6, 7, 8, 9, 10)). Again, we compute the reduced density matrix

$$\hat{\rho}_{A_2} = \text{tr}_{B_2} \hat{\rho}_0, \quad (63)$$

and find its eigenvectors, which we denote $\{|\psi_{i_2}^{A_2}\rangle\}$.

We continue dividing the system until the end (in our example, we go up to A_5). The final, ground state-optimized k -local measurement basis is then given by

$$\{|\psi_{i_1}^{A_1}\rangle \otimes |\psi_{i_2}^{A_2}\rangle \otimes |\psi_{i_3}^{A_3}\rangle \otimes |\psi_{i_4}^{A_4}\rangle \otimes |\psi_{i_5}^{A_5}\rangle\}. \quad (64)$$

2. Observable-optimized measurements, type 1

Second, we introduce a method that is k -local optimization for a specific observable, in our case the Hamiltonian.

The motivation behind this optimization is that the estimation of the mean value of observable works better the more the measurement resembles the eigenbasis of the observable. Thus, we create a procedure that generates a measurement that somewhat resembles the estimated observable.

We illustrate this method on the Heisenberg model, assuming $L = 10$, which is given by the Hamiltonian (assuming hard-wall boundary conditions)

$$\hat{H} = \sum_{i=1}^9 (\hat{\sigma}_i^x \hat{\sigma}_{i+1}^x + \hat{\sigma}_i^y \hat{\sigma}_{i+1}^y + \hat{\sigma}_i^z \hat{\sigma}_{i+1}^z) + \sum_{i=1}^{10} h_i \hat{\sigma}_i^z. \quad (65)$$

For $k = 1$ -local measurement, we take out all the terms that span more than a single site. This leads to a modified Hamiltonian

$$\hat{H}_1 = \sum_{i=1}^{10} h_i \hat{\sigma}_i^z. \quad (66)$$

We call the eigenbasis of this Hamiltonian the $k = 1$ -local observable optimized measurement for the Hamiltonian.

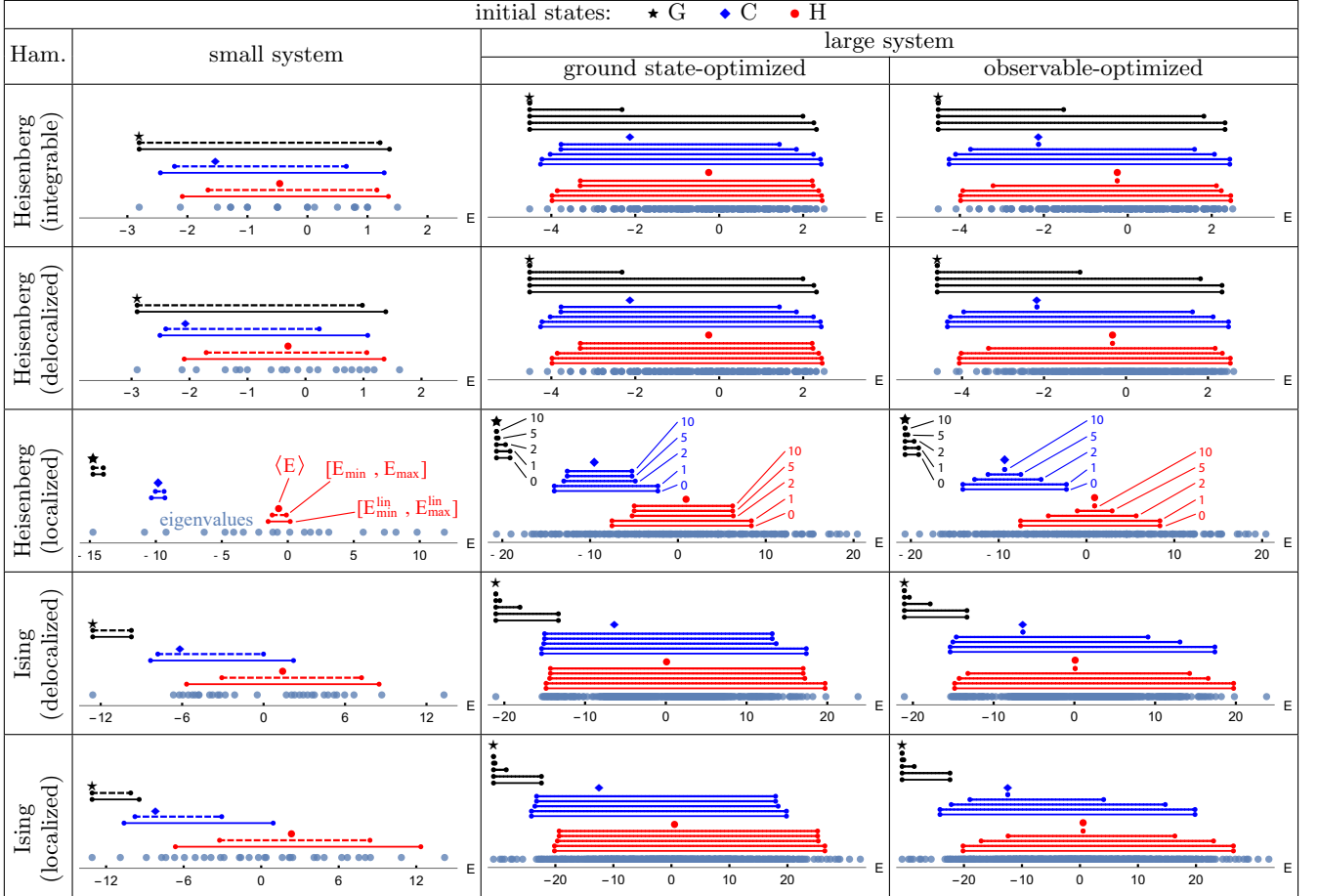


TABLE II. Estimating energy with the local number and k -local optimized measurements, for various Hamiltonians and sizes of Hilbert space delineated in Table I. The initial state is either a ground state (G), a pure thermal state (C - cold), Eq. (25) in the main text, or a state drawn randomly from the Hilbert space with the Haar measure (H - hot). Small systems (left panel): the graphs show the true mean energy $\langle E \rangle$ (single symbol), intervals $[E_{\min}^{\text{lin}}, E_{\max}^{\text{lin}}]$ (full-line) and $[E_{\min}, E_{\max}]$ (dashed-line), for each state ordered from top to bottom, and the list of energy eigenvalues at the very bottom. Large systems: the true mean energy $\langle E \rangle$ (single symbol), intervals $[E_{\min}^{(k)}, E_{\max}^{(k)}]$ (full-lines), denoting analytic bounds computed for k -local measurements, $k = 0, 1, 2, 5, 10$ (see Fig. 5), using ground state-optimized method (middle panel), and observable-optimized type 1 method (right panel). See the observable-optimized type 2 method for the PXP model in Fig. 7. **Observations:** 1) There is little difference between the integrable and delocalized phases of the Heisenberg model in the estimation of energy. Bethe integrability does not seem to play a role. 2) Estimation of energy in the localized phase of the Heisenberg model works well for both small and large systems. It managed to exclude $Q_1 = 97.5\%$ of the range of energies when estimating the ground state energy using two-qubit ($k = 2$) measurements. This is due to a large overlap between energy eigenstates and the local number basis. 3) Estimation of the ground state energy in the Ising model works well both in the localized ($Q_1 = 96.7\%$ for $k = 2$) and delocalized ($Q_1 = 92.9\%$ for $k = 2$) phases. This is due to the low entanglement in the ground state. See the continuation of this Table in Table III.

Incidentally, in this case, this basis is exactly the same as the computational basis.

For $k = 2$ -local measurement, we divide the lattice into blocks of two sites and take out all the terms that cross those blocks. This leads to

$$\hat{H}_2 = \sum_{i=1,3,5,7,9} (\hat{\sigma}_i^x \hat{\sigma}_{i+1}^x + \hat{\sigma}_i^y \hat{\sigma}_{i+1}^y + \hat{\sigma}_i^z \hat{\sigma}_{i+1}^z) + \sum_{i=1}^{10} h_i \hat{\sigma}_i^z. \quad (67)$$

The eigenbasis of this Hamiltonian is the $k = 2$ -local observable optimized measurement for the Hamiltonian.

For $k = 5$ -local measurement, we divide the lattice into two blocks of five sites and take out all the terms that

cross those blocks. This leads to

$$\hat{H}_5 = \sum_{i=1, \dots, 4, 6, \dots, 9} (\hat{\sigma}_i^x \hat{\sigma}_{i+1}^x + \hat{\sigma}_i^y \hat{\sigma}_{i+1}^y + \hat{\sigma}_i^z \hat{\sigma}_{i+1}^z) + \sum_{i=1}^{10} h_i \hat{\sigma}_i^z. \quad (68)$$

The eigenbasis of this Hamiltonian is the $k = 5$ -local observable optimized measurement for the Hamiltonian.

The case of $k = 10$ -local measurement, the corresponding Hamiltonian is the original Hamiltonian itself,

$$\hat{H}_{10} = \hat{H}. \quad (69)$$

Measuring in the basis of this Hamiltonian is the same

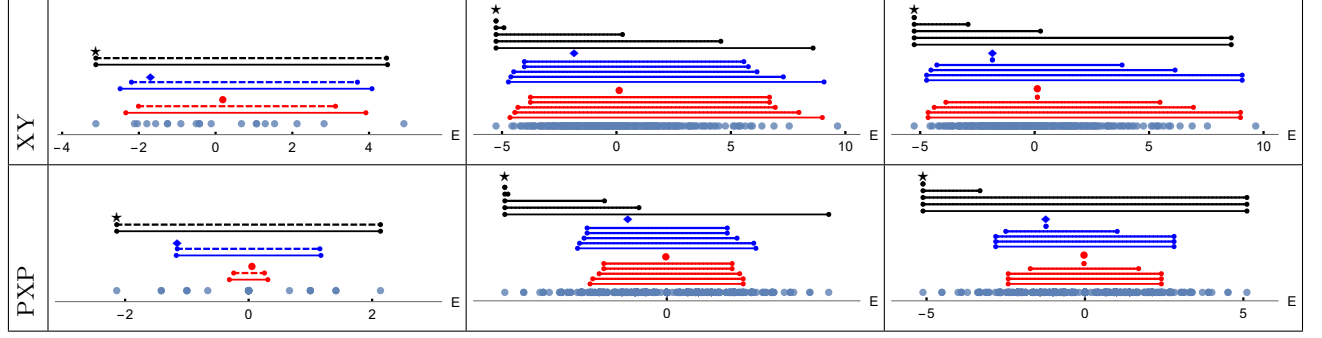


TABLE III. 4) In the XY and PXP models, the local particle number measurement ($k = 0$) does not determine the ground state energy well. This is because low and high-energy eigenstates produce similar, or the same in the case of PXP, distribution of outcomes. 5) Estimation of the hot state energy in the PXP model works significantly better than estimating the ground state energy. This is because of the high degeneracy in the middle of the spectrum. 6) The ground state-optimized method performs better for ground states than the observable-optimized method, but it performs worse on average.

as measuring the Hamiltonian itself, which yields perfect precision in the estimation of its mean value.

3. Observable-optimized measurements, type 2

Alternatively, one can consider a different way of finding observable-optimized measurements, somewhat similar to the state optimization in subsection [VB1](#). For $k = 2$ and $L = 10$, divide the system into system A_1 (the first two sites (1, 2)) and system B_1 (the last $L - k$ sites (3, 4, 5, 6, 7, 8, 9, 10)). Then compute the “reduced Hamiltonian”

$$\hat{H}^{A_1} = \text{tr}_{B_1} \hat{H}, \quad (70)$$

and diagonalize it, obtaining its eigenbasis $\{|\psi_{i_1}^{A_1}\rangle\}$. Continue analogously as in subsection [VB1](#) to generate the global observable-optimized basis for $k = 2$,

$$\{|\psi_{i_1}^{A_1}\rangle \otimes |\psi_{i_2}^{A_2}\rangle \otimes |\psi_{i_3}^{A_3}\rangle \otimes |\psi_{i_4}^{A_4}\rangle \otimes |\psi_{i_5}^{A_5}\rangle\}. \quad (71)$$

In our numerical experiments, due to the specific forms of the Hamiltonian, type 1 and type 2 observable-optimized measurements differ only in the PXP model. See Fig. 7.

4. Generating the unitary

Finally, we want to transform the optimized measurement and express it as a combination of a unitary operator applied on the state of the system, and after that measuring in the computational basis. This is illustrated in Fig. 6. Assuming again our example $k = 2$ and $L = 10$, we start deriving the formula for U^{A_1} with requiring that the probability of outcome is the same in both situations:

$$\langle j_1, j_2 | U^{A_1} \hat{\rho} U^{A_1\dagger} | j_1, j_2 \rangle = \langle \psi_{i_1}^{A_1} | \hat{\rho} | \psi_{i_1}^{A_1} \rangle, \quad (72)$$

where $|j_1, j_2\rangle$ is the computational basis vector, $|\psi_{i_1}^{A_1}\rangle$ an optimized basis vector on the first two sites, and we want to match each couple j_1, j_2 to one i_1 . A sufficient condition is

$$|\psi_{i_1}^{A_1}\rangle = U^{A_1\dagger} |j_1, j_2\rangle \quad (73)$$

Assuming that $|\psi_{i_1}^{A_1}\rangle$ is a column vector written in the computational basis, and that each site is a qubit (which leads to $i_1 = 1, 2, 3, 4$), we have

$$U^{A_1\dagger} = \begin{pmatrix} |\psi_1^{A_1}\rangle & |\psi_2^{A_1}\rangle & |\psi_3^{A_1}\rangle & |\psi_4^{A_1}\rangle \end{pmatrix}. \quad (74)$$

This means that

$$U^{A_1} = \begin{pmatrix} |\psi_1^{A_1}\rangle^\dagger \\ |\psi_2^{A_1}\rangle^\dagger \\ |\psi_3^{A_1}\rangle^\dagger \\ |\psi_4^{A_1}\rangle^\dagger \end{pmatrix} = \begin{pmatrix} \langle \psi_1^{A_1} | \\ \langle \psi_2^{A_1} | \\ \langle \psi_3^{A_1} | \\ \langle \psi_4^{A_1} | \end{pmatrix}. \quad (75)$$

The global optimized measurement then consists of applying the unitary operation

$$U = U^{A_1} \otimes \dots \otimes U^{A_5} = \begin{pmatrix} \langle \psi_1^{A_1} | \\ \langle \psi_2^{A_1} | \\ \langle \psi_3^{A_1} | \\ \langle \psi_4^{A_1} | \end{pmatrix} \otimes \dots \otimes \begin{pmatrix} \langle \psi_1^{A_5} | \\ \langle \psi_2^{A_5} | \\ \langle \psi_3^{A_5} | \\ \langle \psi_4^{A_5} | \end{pmatrix} \quad (76)$$

on the system and then measuring in the computational basis.

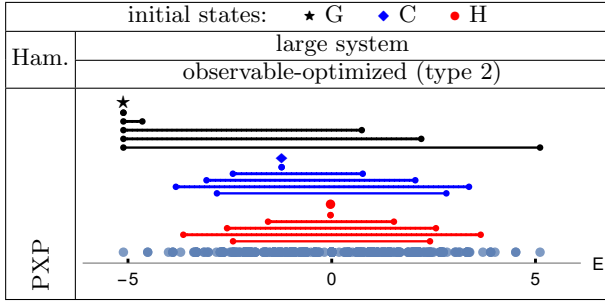


FIG. 7. Observable-optimized type 2 method for the large system of the PXP model. The PXP model is the only of our considered models in which type 1 and type 2 differ. Notice the worse performance for $k = 1$ compared to $k = 0$ for the cold and hot states, but also better performance for $k = 1, 2$ compared to the type 1 method for the ground state.